| Author(s)/Höf.: | Benedikt Ómarsson, Ragnar Bjornsson and Oddur Ingólfsson |

| Title/Titill: | Proton Shuttling and Reaction Paths in Dissociative Electron Attachment to Ortho- and Paratetrafluorohydroquinone, an Experimental and Theoretical Study |

Please cite the original version:

Vinsamlega vísið til útgefnu greinarinnar:

Ómarsson, B., Bjornsson, R., & Ingólfsson, O. (2017). Proton Shuttling and Reaction Paths in Dissociative Electron Attachment to o- and p-Tetrafluorohydroquinone, an Experimental and Theoretical Study. *The Journal of Physical Chemistry A, 121*(30), 5580-5585. doi:10.1021/acs.jpca.7b05010

Proton Shuttling and Reaction Paths in Dissociative Electron Attachment to Ortho- and Para-tetrafluorohydroquinone, an Experimental and Theoretical Study

Benedikt Ómarsson[‡]*, Ragnar Bjornsson*[‡] *and Oddur Ingólfsson*[‡]*

[‡] Science Institute and Department of Chemistry, University of Iceland, Dunhagi 3, 107

Reykjavík, Iceland.

Corresponding Author

*E-mail: odduring@hi.is.

ABSTRACT

Here we present a combined experimental and theoretical study on the fragmentation of *ortho*-and *para*-tetrafluorohydroquinone upon low energy electron attachment. Despite an identical ring-skeleton and identical functional groups in these constitutional isomers, they show distinctly different fragmentation patterns, a phenomenon that cannot be explained by distinct resonances or different thermochemistry. Using high-level quantum chemical calculations with the computationally affordable domain localized pair natural orbital approach, DLPNO-CCSD(T), we are able to provide a complete and accurate description of the respective reaction dynamics, revealing proton shuttling and transition states for competing channels as the explanation for the different behavior of these isomers. The results represent a "schoolbook example" of how the combination of experiment and modern high-level theory may today provide a thorough understanding of complex reaction dynamics by computationally affordable means.

Introduction

Low energy electrons are ubiquitous in nature and through resonant attachment they may cause destabilization, rearrangement and extensive fragmentation of large and complex molecular systems - processes termed dissociative electron attachment (DEA)[1]. Such processes play an important role in a variety of areas including radiation damage to biological systems[2,3,4], nano-fabrication using high-energy electron beams[5,6] or extreme ultraviolet lithography[7] and in plasma processing[8]. Currently experimental studies on such processes are, however, mainly limited to their energy-dependency, efficiency, and fragment identification, though lately, studies on the angular dependency of the DEA process have been more apparent, enabled through recent instrumental development (see e.g., ref[9] and refs. therein). Detailed theoretical work of DEA has been pursued by a few groups where it has been found that a complete description of the attachment process requires inclusion of coupling of the electronic states to the free electron continuum to describe metastable states as well as accounting for nuclear dynamics[9,10,11].

Quantum chemical calculations of bound anion potential energy surfaces are also commonly used to support interpretation of product formation in DEA based on the thermochemistry of the respective processes. Open-shell anions and anionic fragments in DEA processes, however, present challenges to contemporary quantum chemistry and the commonly employed density functional theory (DFT) methodology typically behaves better for closed-shell systems; there have been notable shortcomings of DFT methods for bond dissociation energies and electron affinities that involve radicals and open-shell anions[12,13,14,15]. Coupled cluster theory, on the other hand, is capable of chemical accuracy (< 1 kcal/mol), including both radicals and anions, provided that a single determinant is a reasonable first approximation of the molecular wavefunction. The CCSD(T) method (coupled cluster singles doubles perturbative triples) has

sometimes been referred to as the gold standard of quantum chemistry[16]. However, due to its severe scaling, $O(N^7)$ with system size, traditional CCSD(T) calculations are simply not feasible for large systems and become out of reach even for moderately sized systems when used in combination with large and diffuse basis sets as required for a good description of anions. With the rise of local correlation approaches in recent years, the restrictive scaling of the CCSD(T) method has been dramatically reduced and is coming close to linear in these local correlation methods, while still capturing 99.9 % of electron correlation of the canonical method. In a previous publication on DEA to a π-$(C_3H_5)Ru(CO)_3Br$ metal complex[17] we found that both GGA and hybrid-GGA density functionals failed to give thermochemical thresholds in agreement with the experimental appearance energies, while for the approximate LPNO-pCCSD/2a coupled cluster method (using the older local pair natural orbital methodology, LPNO) this was not the case.

The domain localized pair natural orbital (DLPNO) approach by Neese and coworkers[18,19,20] has very recently become available for open-shell systems[21] in the ORCA 4.0 quantum chemistry code, extending the use of the affordable DLPNO-CCSD(T) method to the chemistry of open-shell organic radicals and anions as well as open-shell transition metal complexes.

In the current contribution we present a combined experimental and theoretical study on the principal DEA pathways in *para-* and *ortho-*tetrafluorohydroquinone (TFHQ), a derivative of quinone - a critical component of the most pervasive redox systems in all living organisms[22]. Despite their almost identical chemical constitution, *o-* and *p-*TFHQ show distinctly different behavior with respect to their principal fragmentation pathways upon low energy electron attachment, an intriguing fact that can not be explained from the thermochemistry of the respective processes or distinct resonances. However, through the calculation of the bound anion

potential energy surfaces, calculated by high-level theory via the affordable DLPNO-CCSD(T) approach, in combination with large and diffuse basis sets (aug-cc-pVTZ, aug-cc-pVQZ) extrapolated to the complete basis set limit (CBS), we are able to reveal distinct chemical barriers as an explanation for this curious behavior, presenting a "schoolbook example" of how the combination of experiment and current theory may allow for detailed understanding of complex reaction dynamics.

Methods

The experimental setup has been described in detail elsewhere[23] and we therefore limit our discussion to a brief description. The experimental setup is a high-vacuum apparatus where an electron beam, formed in a trochoidal electron monochromator crosses an effusive molecular beam. The solid samples are sublimed into the vacuum chamber through an inlet system maintained at 60 °C and the monochromator is held at a constant temperature of 120 °C. In the experiments, we assume the gas to be in thermal equilibrium to the inlet system. The base pressure for this setup is on the order of 10^{-8} mbar and the working pressure was maintained at approximately 5×10^{-7} mbar. Anionic fragments formed through DEA are extracted by a weak (~1 V/cm) electric field towards a HIDEN EPIC 1000 quadrupole mass spectrometer (Hiden analytical, Warrington UK). The electron energy scale was calibrated with respect to the formation of SF_6^- from SF_6 at ≈ 0 eV and the incident electron energy resolution (120-140 meV) is estimated from the FWHM of the SF_6^- signal. The compound p-TFHQ was purchased from Sigma-Aldrich (St. Louis, MO, USA) with a stated purity of 97 %. The compound o-TFHQ was purchased from Fluorochem (Hadfield, Derbyshire, UK) with a stated purity of 97 %. Both compounds are solids at room temperature and were used as delivered.

Quantum chemical calculations were carried out using the ORCA program[24], version 3.0.3 (DFT calculations) and version 4.0.0 (coupled cluster calculations). ORCA interfaced with Chemshell, version 3.63[25,26] was used for saddle-point searches, using the DL-FIND optimization program[27] in Chemshell and the nudged elastic band (NEB) method[28,29,30,31]. Approximate saddle points were first found using NEB and then located more accurately by the eigenvalue-following method in ORCA and confirmed as first-order saddle-points by exact Hessian calculations. All geometry optimizations and saddle-point optimizations were performed using the B3LYP[32,33,34] hybrid density functional with the ma-def2-TZVP basis set[35,36] (minimally augmented diffuse def2-TZVP basis set). All stationary points were confirmed by Hessian calculations at the same level and zero-point vibrational energy contributions were included in all reported energies. Higher level single-point energy calculations were performed on B3LYP/ma-def2-TZVP geometries using the wavefunction theory method, DLPNO-CCSD(T)[18,19,20,21]. Calculations were performed using aug-cc-pVTZ and aug-cc-pVQZ basis sets[37] and the HF energies and correlation energies were extrapolated to the complete basis set limit (CBS) using the automatic procedure in ORCA[38]. Quasi-restricted orbitals (QROs)[39] were used as a reference determinant from the UHF orbitals that reduces spin contamination in the coupled cluster calculations.

Results and discussion

Figure 1 shows the ion yield curves for the principal fragmentation pathways observed from *p*-TFHQ (left) and *o*-TFHQ (right) upon electron attachment in the energy range from about 0 to 15 eV. These constitute the loss of a hydrogen fluoride unit (top panels), the loss of two hydrogen fluoride units (middle panels) and the loss of a hydrogen fluoride and a CO unit (bottom panels). *Id est*, the formation of $[M - HF]^-$, $[M - 2HF]^-$ and $[M - HF - CO]^-$. In addition a significant number of lower intensity fragments are observed from these compounds,

but we will discuss these elsewhere. The main contributions from the principal fragments in the respective ion yield curve shown in Fig. 1 are through two low-lying resonances exhibited through maxima close to 0 eV and around 1 to 1.5 eV in the respective ion yield curves. Here we exercise the practice of Jordan et al.[40,41] and we label the orbitals according to the C_{2v} point group, thus associating the 0 eV contribution with a single electron occupation of the lowest lying $a_2(\pi^*)$ orbital. The resonance leading to the contributions peaking between 1 and 1.5 eV in the ion yield curves we assign as a $^2B_1$ shape resonance, associated with the $b_1(\pi^*)$ orbital.
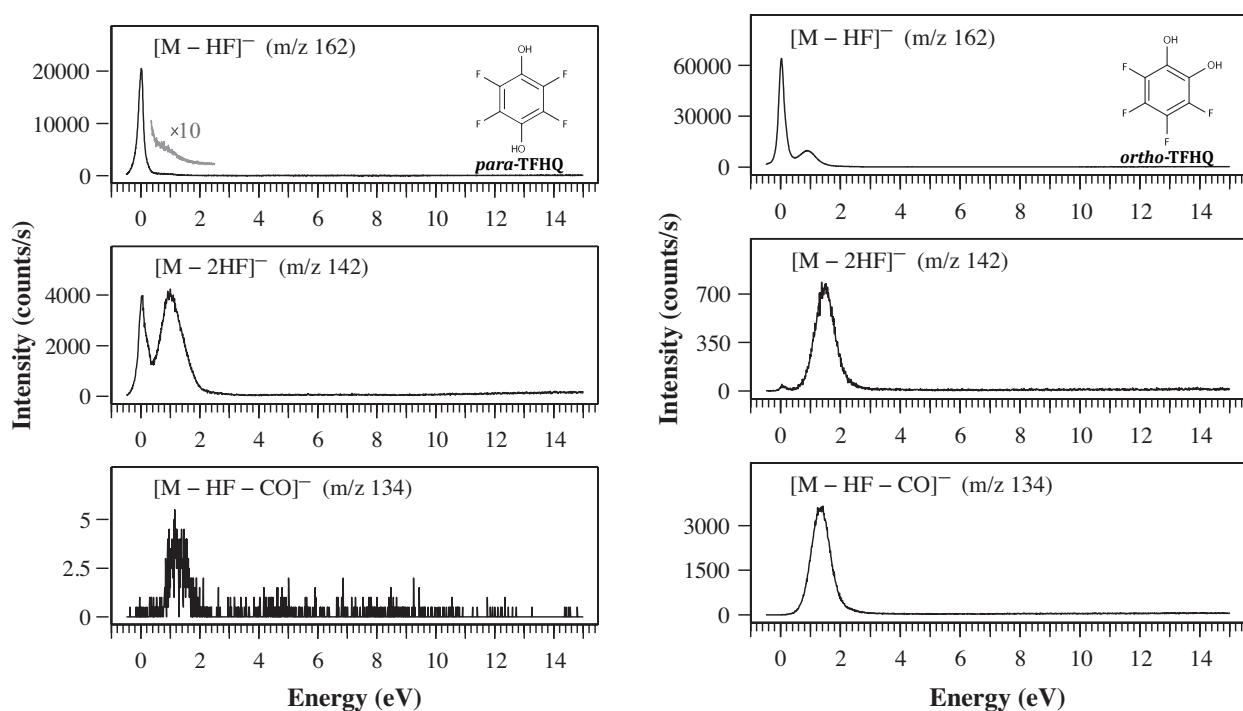

Figure 1. Selected ion yield curves observed in DEA to *p*-TFHQ (left) and *o*-TFHQ (right).

For both *p*-TFHQ and *o*-TFHQ the most intense contribution is that of the formation of $[M - HF]^-$ i.e., the loss of one HF unit, which proceeds primarily through the 0 eV resonance. For *o*-TFHQ, however, a significant contribution through the higher-lying $^2B_1$ resonance is also observed at around 1 eV.
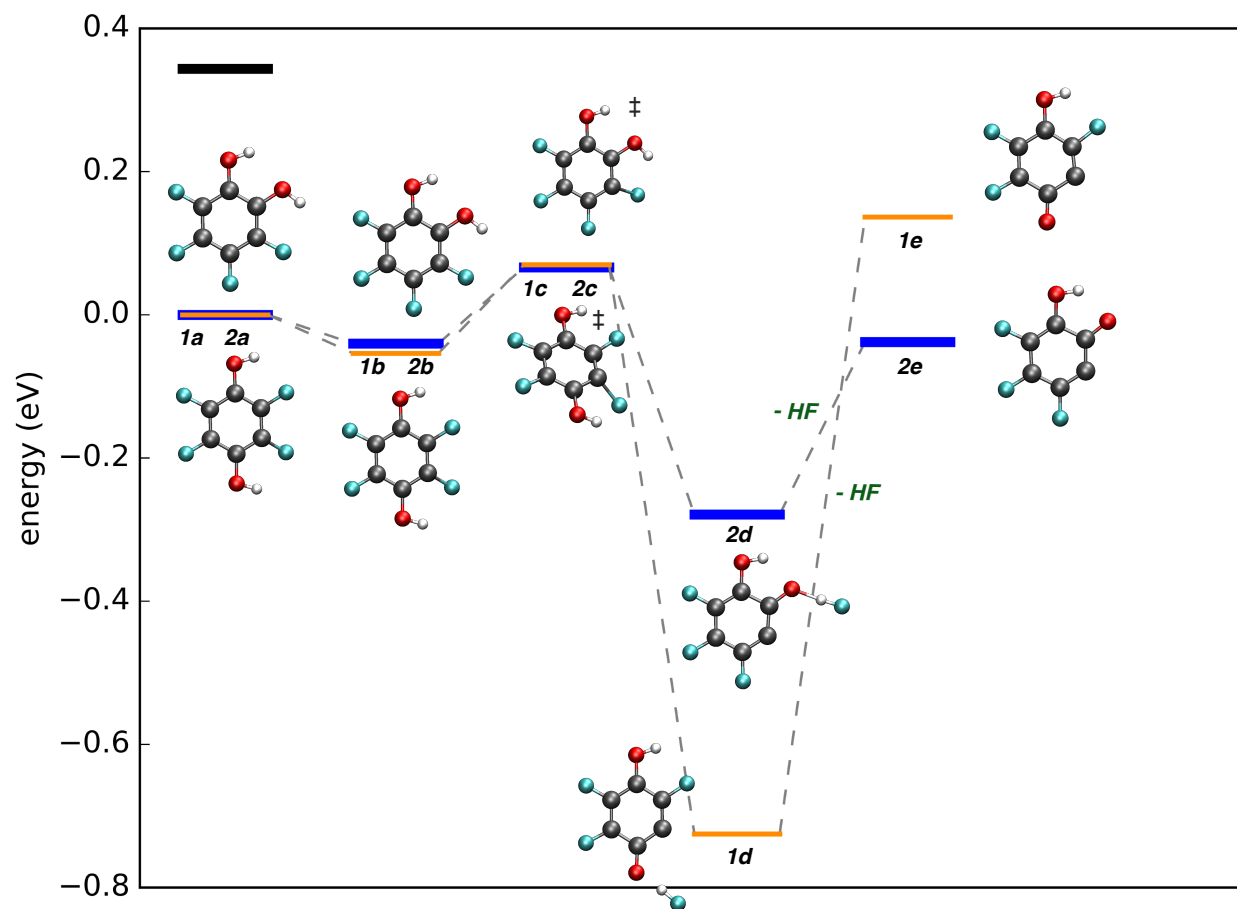
Figure 2. Calculated reaction paths (DLPNO-CCSD(T)/CBS level of theory) for the first hydrogen fluoride loss from both *p*-TFHQ (**1a**) and *o*-TFHQ (**2a**). The parent anions are labeled **1b** and **2b**. The black bar denotes the 0.34 eV thermal energy available at the 333 K experimental temperature and ‡ denotes a saddle point.

Figure 2 compares reaction-profile diagrams for the loss of hydrogen fluoride from *p*-TFHQ and *o*-TFHQ derived from single-point DLPNO-CCSD(T)/CBS calculations on the respective B3LYP/ma-def2-TZVP optimized structures. The total energy of the neutral precursors **1a** and **2a** is set as 0 eV, and the relative energies for all depicted reaction steps are tabulated in Tables S1-S2 in the supporting information. All energies include zero-point energy corrections calculated at the B3LYP/ma-def2-TZVP level of theory. The black bar on the far left in Figure 2 signifies the internal (vibrational, rotational and translational) energy (0.34 eV) of the neutral

molecule under the current experimental conditions at 333 K (temperature of the inlet system). At this level of theory the electron affinity of *p*-TFHQ and *o*-TFHQ is found to be 0.05 eV and 0.04 eV respectively, For *p*-TFHQ and *o*-TFHQ the reaction path leading to the loss of one HF unit proceeds from the molecular anion (**1b** and **2b**) through an insignificant barrier (**1c** and **2c**) to form an intermediate where the departing HF is still hydrogen-bonded to the respective oxygen from which the hydrogen originates (**1d** and **2d**). This intermediate then decays through detachment of the hydrogen fluoride forming the anion [M − HF]⁻ (**1e** and **2e**). For *p*-TFHQ this channel is endothermic by about 137 meV and for *o*-TFHQ it is exothermic by 38 meV. Hence, under the current experimental conditions, at 333K, the HF loss is readily accessible for both compounds at 0 eV incident electron energies. This is reflected in the high intensity 0 eV contributions in the [M − HF]⁻ ion yields shown in the top panels of Figure 1. However, the significant production of [M − HF]⁻ through the higher lying resonance in *o*-TFHQ as compared to the lack of [M − HF]⁻ formation through this resonance in *p*-TFHQ is not readily explainable from these considerations alone.

Turning back to Figure 1 it is apparent that the loss of the second HF unit, i.e., the formation of [M − 2HF]⁻ from *p*-TFHQ is readily accessible at 0 eV as well as through the higher energy resonance, while the [M − 2HF]⁻ from *o*-TFHQ is restricted to the higher energy resonance. Conversely, the loss of one HF and one CO unit i.e., the formation of [M − HF − CO]⁻, is practically absent in *p*-TFHQ while it is significant through the higher lying resonance in *o*-TFHQ.
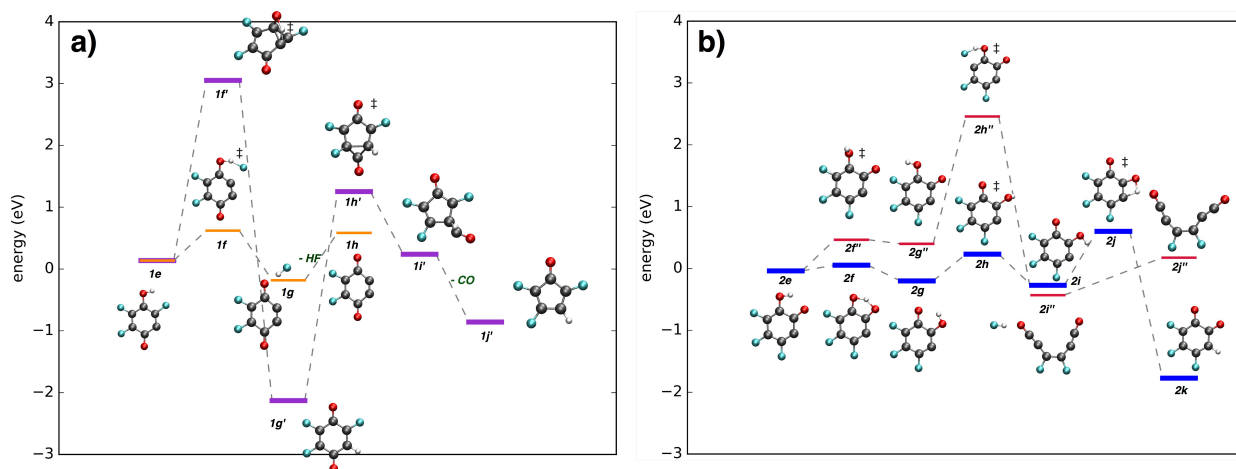
Figure 3. a) Calculated reaction profile for *p*-TFHQ for the direct 2nd HF elimination to form the cyclic structure **1h** (orange lines), compared to the unfavorable proton-transfer pathway to form the valence-saturated intermediate **1g'** followed by a CO elimination to form the 5-membered ring **1j'** (purple lines). Both paths start from the intermediate **1e** and energies are relative to **1a**. b) Calculated reaction profile for *o*-TFHQ for direct 2nd HF elimination to form the linear structure **2j''** (red lines) compared to proton-shuttling leading to the valence-saturated intermediate **2k** (blue lines). Both paths start from the intermediate **2e** and energies are relative to **2a**. The black bar denotes the 0.34 eV thermal energy available at the 333 K experimental temperature and ‡ denotes the saddle points.

In Figure 3a the calculated reaction-profile diagrams for the formation of [M − 2HF]⁻ (orange lines) and [M − HF − CO]⁻ (purple lines) are compared for *p*-TFHQ for the whole reaction path. Figure 3b shows the calculated reaction-profile diagram for the direct formation of [M − 2HF]⁻ from *o*-TFHQ (red lines) along with a proton shuttling pathway leading to an intermediate on the way to [M − HF − CO]⁻ from *o*-TFHQ (blue lines). For clarity, the reaction-profile diagram for the actual formation of [M − HF − CO]⁻ from this intermediate is shown separately in Figure 4 (blue lines) along with the path describing the loss of the second HF from the same intermediate (red lines); i.e. a second, more favorable path for the [M − 2HF]⁻ formation from *o*-TFHQ. In both *p*-TFHQ and *o*-TFHQ the initial HF elimination has left an unsaturated carbon next to the dehydrogenated oxygen, however, in *p*-TFHQ this oxygen is in a *para* position to the remaining

intact hydroxyl group while in *o*-TFHQ it is in an *ortho* position. Proton shuttling from the hydroxyl group over the highly electronegative, dehydrogenated oxygen to the unsaturated carbon is thus a fairly straightforward path with comparatively low-lying transition states. This is clear from Figure 3a which shows that in *o*-TFHQ the highest barrier on the path to this intermediate is associated with the transfer of the hydrogen to the unsaturated carbon (**2j)**. This barrier is about 0.6 eV. Comparable proton shuttling is simply not possible in *p*-TFHQ and direct hydrogen transfer from the hydroxyl group to the unsaturated carbon over the ring requires considerably more energy. The lowest transition state we find for this transfer (**1f'**) is more than 3 eV above the total energy of the neutral. Conversely the highest barrier for a second HF loss from *p*-TFHQ is close to 0.6 eV (**1f**) while the highest barrier for the second HF loss from *o*-TFHQ is 2.5 eV (**2h''**). This gives a complete picture of the fragmentation paths for *p*-TFHQ, whereby we attribute the 0 eV contribution in the [M − 2HF]⁻ yield to the high-energy portion of the Maxwell Boltzmann internal energy distribution at the current experimental temperature. Furthermore, the low barrier for the second HF loss from *p*-TFHQ reduces the lifetime of [M − HF]⁻ with regards to further fragmentation (to form [M − 2HF]⁻) which explains the lack of the observation of [M − HF]⁻ from *p*-TFHQ through the higher energy resonance as compared to *o*-TFHQ where the direct loss of the second HF is impeded due to the high activation barrier (2.5 eV).

To explain the formation of [M − 2HF]⁻ and [M − HF − CO]⁻ from *o*-TFHQ through the higher lying resonance, however, we have computed the reaction path from the intermediate **2k** to these fragments (**2n** and **2n'** respectively). The calculated reaction-profile diagrams are shown in Figure 4.
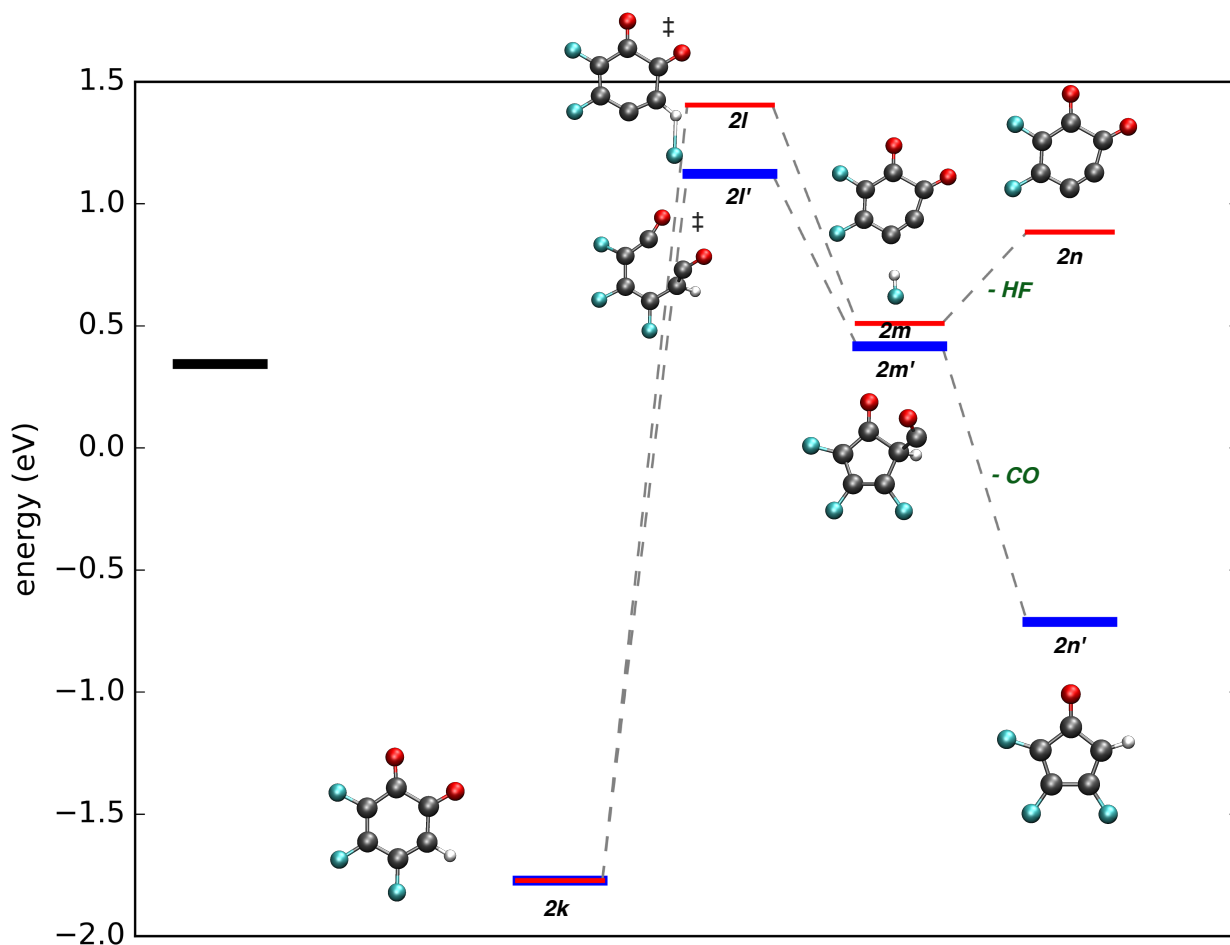
Figure 4. Calculated reaction profile for *o*-TFHQ from intermediate **2k** (purple line) leading to either 2nd HF elimination and product **2n** (red lines) or CO elimination and 5-membered ring product **2n'** (blue lines). The black bar denotes the 0.34 eV thermal energy available at the 333 K experimental temperature and ‡ denotes the saddle points.

We find that the highest barrier on the CO loss path (blue lines) is that of the ring opening which amounts to about 1.1 eV. For the second HF loss (red lines) the highest-lying transition state represents the C-F bond rupture and is 1.4 eV above the neutral ground state. This resonates well with the observed ion yield for both these fragments, which are only observed through the higher lying resonance, but with appreciable intensities. Furthermore, in accordance with the higher reaction barrier, the formation of [M − 2HF]⁻ is less efficient than the [M − HF −

CO]$^-$ formation from o-TFHQ and the [M $-$ 2HF]$^-$ ion yield is shifted to slightly higher energies. Considering the experimental temperature and the Maxwell Boltzmann internal energy distribution, the match of the experimental appearance with the calculated barriers is very good and the different product formation for p-TFHQ as compared to o-TFHQ can be traced back to distinct transition states along the multi-intermediate reaction pathways, giving a complete picture of the dynamics of these processes. For clarity, an overview of the complete reaction pathways for both p-TFHQ and o-TFHQ is given in figure 5.
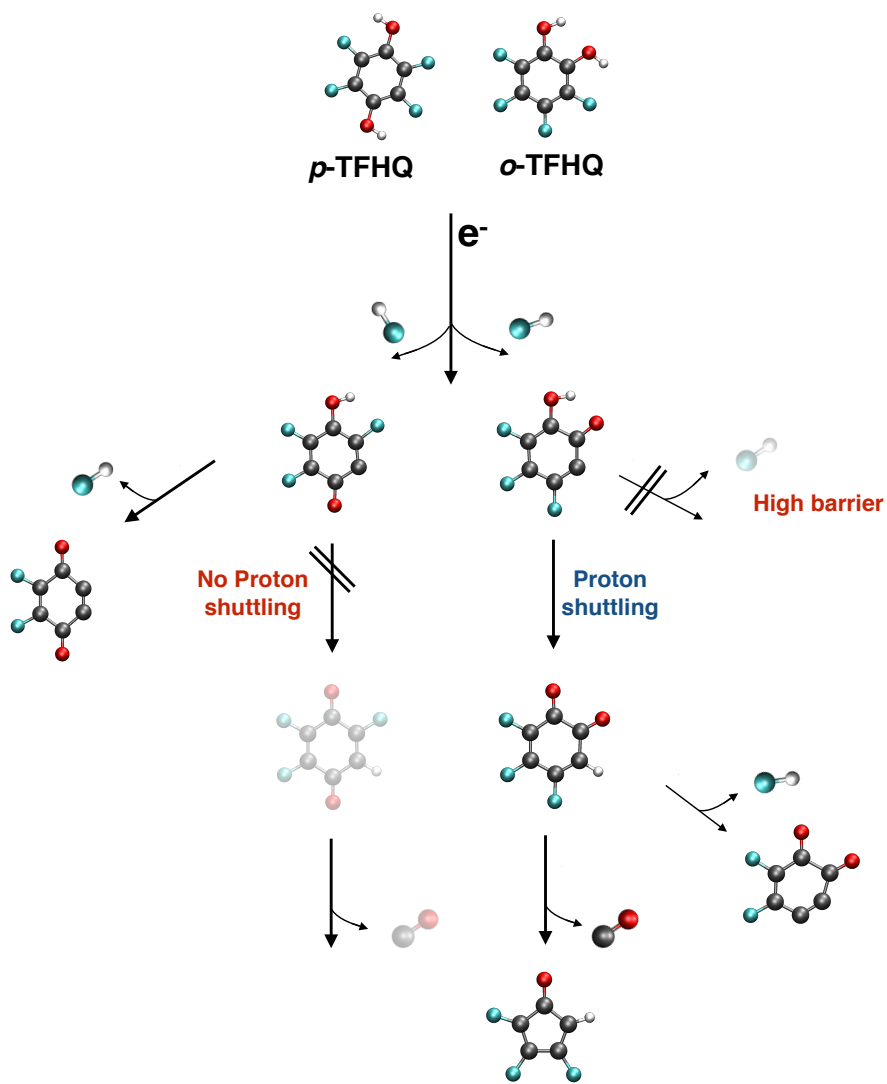

Figure 5. Overview of the different fragmentation pathways for o-TFHQ vs. p-TFHQ.

Conclusions

In conclusion, a complete description of the reaction paths for complex rearrangement reactions in DEA to *p*-TFHQ vs. *o*-TFHQ were computed at the DLPNO-CCSD(T) level of theory, offering a consistent and complete explanation of the experimental observations. Both *p*-TFHQ and *o*-TFHQ initially lose a single HF unit through a close to barrier-free path, forming [M − HF]⁻ with high efficiency close to 0 eV electron incident energy. The barrier for direct loss of the second HF unit from *p*-TFHQ is only about 0.6 eV while the second HF loss from *o*-THFQ is associated with a considerable barrier of about 2.5 eV. This enables direct formation of [M − 2HF]⁻ from *p*-TFHQ through the higher lying resonance demonstrated by significant contribution in the ion yield at around 1-2 eV. The loss of a second HF from *o*-TFHQ, on the other hand, requires further rearrangement at these energies. This situation is also apparent in the lack of the observation of [M − HF]⁻ through the higher lying resonance in *p*-TFHQ where the competing second HF loss may be considered a direct path. Conversely, for *o*-TFHQ, where the barrier for the *direct* second HF loss is about 2.5 eV, further fragmentation to form [M − 2HF]⁻ is impeded. For *o*-TFHQ, however, a low energy proton shuttling pathway from [M − HF]⁻, with a reaction barrier of only 0.6 eV, is favorable through the higher energy resonance. This proton shuttling pathway, in turn, leads to an intermediate from which both [M − 2HF]⁻ and [M − HF − CO]⁻ may form. The highest reaction barriers for these pathways are 1.1 and 1.4 eV respectively, which is reflected in the efficiency and energy dependency of these channels in the respective ion yield curves. The good agreement with the experimental results and the completeness of the description clearly demonstrates how the combination of high-level quantum chemistry and experiment may offer a comprehensive picture of the dynamics behind complex reactions involving extensive fragmentation and new bond formation.

ASSOCIATED CONTENT

Supporting Information.

Reaction energies for all steps in Figures 2-4 included as Tables S1-S2 .

AUTHOR INFORMATION

Notes

The authors declare no competing financial interests.

ACKNOWLEDGMENT

References

[1] Bald, I.; Langer, J.; Tegeder, P.; Ingólfsson, O. From isolated molecules through clusters and condensates to the building blocks of life. *Int. J. Mass Spectrom.* **2008**, *277*, 4-25.

[2] Boudaïffa, B.; Cloutier, P.; Hunting, D.; Huels, M. A.; Sanche, L. Resonant formation of DNA strand breaks by low-energy (3 to 20 eV) electrons. *Science,* **2000**, *287*, 1658-1660.

[3] Baccarelli, I.; Bald, I.; Gianturco, F. A.; Illenberger, E.; Kopyra, Electron-induced damage of DNA and its components: Experiments and theoretical models, *J. Phys. Rep.* **2011**, *508*, 1-44.

[4] Sanche, L. Low energy electron-driven damage in biomolecules. *Eur. Phys. J. D* **2005**, *35*, 367-390.

[5] Thorman, R. M.; Ragesh Kumar, T. P.; Fairbrother, D. H.; Ingólfsson, O. The role of low-

energy electrons in focused electron beam induced deposition: four case studies of representative precursors. *Beilstein J. Nanotechnol*. **2015,** *6*, 1904-1926.

[6] Silvis-Cividjian, N.; Hagen, C.; Leunissen, L.; Kruit, P. The role of secondary electrons in electron-beam-induced-deposition spatial resolution. *Microelectron. Eng*. **2002**, *61*, 693-699.

[7] Bhattarai, S.; Neureuther, A. R.; Naulleau, P. P. Study of energy delivery and mean free path of low energy electrons in EUV resists, Proc. SPIE: **2016**; pp 97790B-97790B-9.

[8] *Electron-Molecule Interactions and Their Applications*; Christophorou, L. G., Ed.; Academic Press: New York, 1984.

[9] Fabrikant, I. I.; Eden, S.; Mason, N. J.; Fedor, J. in *Advances in atomic, molecular, and optical physics*, Arimondo, E.; Lin, C. C.; Yelin, S. F. Eds., (Academic Press), 2017, vol. 66, pp. 545-657.

[10] *Low-energy Electron Scattering from Molecules, Biomolecules and Surfaces;* Čaŕsky,P.; Čurík, R., Eds.; CRC Press (Taylor and Francis Group): Boca Raton, FL, 2012; pp 161– 230.

[11] Hotop, H.; Ruf, M.-W.; Allan, M.; Fabrikant, I. I. in *Advances in atomic, molecular, and optical physics*, Bederson, B.; Walther, H. Eds., (Academic Press), 2003, vol. 49, pp. 85-216.

[12] Izgorodina, E. I.; Coote, M. L.; Radom, L. Trends in R-X bond dissociation energies (R = Me, Et, i-Pr, t-Bu; X = H, CH3, OCH3, OH, F): a surprising shortcoming of density functional theory. *J. Phys. Chem. A* **2005**, *109*, 7558-7566.

[13] Izgorodina, E. I.; Brittain, D. R.; Hodgson, J. L.; Krenske, E. H.; Lin, C. Y.; Namazian, M.; Coote, M. L. Should contemporary density functional theory methods be used to study the thermodynamics of radical reactions? *J. Phys. Chem. A* **2007**, *111*, 10754-10768.

[14] Jensen, F. Describing anions by density functional theory: fractional electron affinity. *J. Chem. Theory Comput*. **2010**, *6*, 2726-35.

[15] Kim, M. C.; Sim, E.; Burke, K. Communication: Avoiding unbound anions in density functional calculations. *J. Chem. Phys*. **2011**, *134*, 171103.

[16] Lee, T. J.; Scuseria, G. E. in *Quantum Mechanical Electronic Structure Calculations with Chemical Accuracy*, S. R. Langhoff Ed. (Kluwer Academic Publishers): Dordrecht, Netherlands, 1995.

[17] Thorman, R. M.; Bjornsson, R.; Ingólfsson, O. Computational study of dissociative electron attachment to π-allyl ruthenium (II) tricarbonyl bromide. *Eur. Phys. J. D* **2016**, *70*, 164.
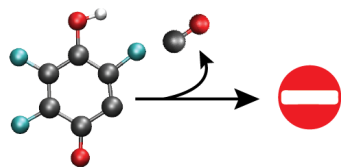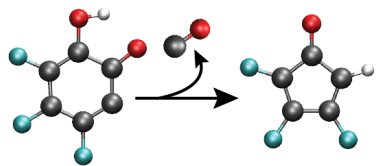
[18] Riplinger, C. Neese, F. An efficient and near linear scaling pair natural orbital based local coupled cluster method. *J. Chem. Phys*. **2013**, *138*, 034106.

[19] Riplinger, C.; Sandhoefer, B.; Hansen, A.; Neese, F. Natural triple excitations in local coupled cluster calculations with pair natural orbitals. *J. Chem. Phys*. **2013**, *139*, 134101.

[20] Riplinger, C.; Pinski, P.; Becker, U.; Valeev, E. F.; Neese, F. Sparse maps-A systematic infrastructure for reduced-scaling electronic structure methods. II. Linear scaling domain based pair natural orbital coupled cluster theory. *J Chem Phys*. **2016**, *144*, 024109.

[21] Saitow, M.; Becker, U.; Riplinger, C.; Valeev, E. F.; Neese, F. A new near-linear scaling, efficient and accurate, open-shell domain-based local pair natural orbital coupled cluster singles and doubles theory, *J. Chem. Phys.* **2017**, *146*, 164105.

[22] Nohl, H.; Jordan, W.; Youngman, R. J. Quinones in biology: functions in electron transfer and oxygen activation. *Adv. Free Radical Bio.* **1986**, *2*, 211-279.

[23] Bjarnason, E. H.; Ómarsson, B.; Engmann, S.; Ómarsson, F. H.; Ingólfsson, O. Dissociative electron attachment to titatinum tetrachloride and titanium tetraisopropoxide. *Eur. Phys. J. D* **2014**, *68*, 121.

[24] Neese, F. The ORCA program system. *WIREs Comput. Mol. Sci.* **2011**, *2*, 73–78.

[25] Metz, S.; Kästner, J.; Sokol, A. A.; Keal, T. W.; Sherwood, P. ChemShell - a modular software package for QM/MM simulations. *WIREs Comput. Mol. Sci.* **2013**, *4*, 101–110.

[26] Sherwood, P.; de Vries, A. H.; Guest, M. F.; Schreckenbach, G.; Catlow, C. R. A.; French, S. A.; Sokol, A. A. ; Bromley, S. T.; Thiel, W.; Turner, A. J. et al. QUASI: A general purpose implementation of the QM/MM approach and its application to problems in catalysis. *J. Mol. Struct.: THEOCHEM.* **2003**, *632*, 1-28.

[27] Kästner, J.; Carr, J. M.; Keal, T. W.; Thiel, W.; Wander, A.; Sherwood, P. DL-FIND: an open-source geometry optimizer for atomistic simulations. *J. Phys. Chem. A* **2009**, *113*, 11856-11865.

[28] Jónsson, H.; Mills, G.; Jacobsen, K. W. Nudged elastic band method for finding minimum energy paths of transitions. *Classical and Quantum Dynamics in Condensed Phase Simulations;* World Scientific, 1998; p. 385-404.

[29] Henkelman, G.; Jónsson, H. Improved tangent estimate in the nudged elastic band method for finding minimum energy paths and saddle points. *J. Chem. Phys.* **2000**, *113*, 9978-9985.

[30] Henkelman, G.; Uberuaga, B. P.; Jónsson, H. A climbing image nudged elastic band method for finding saddle points and minimum energy paths. *J. Chem. Phys.* **2000**, *113*, 9901-9904.

[31] Goumans, T.; Catlow, C.; Brown, W.; Kästner, J.; Sherwood, P. An embedded cluster study of the formation of water on interstellar dust grains. *Phys. Chem. Chem. Phys.* **2009**, *11*, 5431–5436.

[32] Becke, A. D. Density-functional thermochemistry. III. The role of exact exchange. *J. Chem. Phys.* **1993**, *98*, 5648-5652.

[33] Lee, C.; Yang, W.; Parr, R. G. Development of the Colle-Salvetti correlation-energy formula into a functional of the electron density. *Phys. Rev. B* **1988**, *37*, 785–789.

[34] Stephens, P. J.; Devlin, F. J.; Chabalowski, C. F.; Frisch, M. J. Ab initio calculation of vibrational absorption and circular dichroism spectra using density functional force fields. *J. Phys. Chem.* **1994**, *98*, 11623–11627.

[35] Weigend, F.; Ahlrichs, R. Balanced basis sets of split valence, triple zeta valence and quadruple zeta valence quality for H to Rn: Design and assessment of accuracy. *Phys. Chem. Chem. Phys.* **2005**, *7*, 3297-3305.

[36] Zheng, J.; Xu, X.; Truhlar, D. G. Minimally augmented Karlsruhe basis sets. *Theor. Chem. Acc.* **2010**, *128*, 295–305.

[37] Dunning, T. H. Gaussian basis sets for use in correlated molecular calculations. I. The atoms boron through neon and hydrogen. *J. Chem. Phys.* **1989**, *90*, 1007-1023.

[38] Neese, F.; Valeev, E. F. Revisiting the atomic natural orbital approach for basis sets: robust systematic basis sets for explicitly correlated and conventional correlated ab initio methods? *J. Chem. Theory Comput.* **2011**, *7*, 33-43.

[39] Neese, F. Importance of direct spin-spin coupling and spin-flip excitations for the zero-field splittings of transition metal complexes: a case study. *J. Am. Chem. Soc.* **2006**, *128*, 10213–10222.

[40] Jordan, K. D.; Michejda, J. A.; Burrow, P. D. The relative stability of alkyl-substituted benzene anions in the gas phase. *J. Am. Chem. Soc.* **1976**, *98*, 1295-1296.

[41] Jordan, K. D.; Michejda, J. A.; Burrow, P. D. Electron transmission studies of the negative ion states of substituted benzenes in the gas phase. *J. Am. Chem. Soc.* **1976**, *98*, 7189-7191.

TOC GRAPHIC